Diffusion of Toluene and Ethylene in ZSM-12 zeolite: Experimental and numerical study

Insaf Daldoul[1], Hicham Chaouki[2], Serge Kaliaguine[3]

[1,3]Department of Chemical Engineering, Université Laval, Québec, Canada, G1V 0A6
[2]Department of Civil Engineering, Université Laval, Québec, Canada, G1V 0A6

Abstract**—** *The Na^+ and Ag^+ forms of ZSM-12 zeolite microporous were used as effective adsorbents for hydrocarbons trap. Diffusion of a single adsorbed component including ethylene as a light molecule or toluene a heavier one inside a narrow one-dimensional channel was studied. Experimental desorption profiles for these two gases desorbing from both Ag-ZSM-12 and Na-ZSM-12 were obtained at very high heating rates comparable with the one observed during the cold start of a combustion engine. Numerical simulation based on Fick's law and a transient diffusion boundary value yielded a good fitting of these experimental results. For both ZSM-12 forms considered in this study, diffusion activation energies E_ω and E_Ξ for toluene are much higher than those for ethylene. The values of these parameters are higher for the Ag^+ exchanged zeolite than for Na-ZSM-12 and related to the presence of strong Lewis acid sites in the former material. In addition each activation energy for Na-ZSM-12 and Ag-ZSM-12 decreases at increasing heating rate. This was explained by thermal vibrations of the zeolite lattice which allow higher diffusivity at high temperature.*

Keywords**— single component, single file diffusion, temperature-programmed desorption, ZSM-12***

I. INTRODUCTION

Faced with increasingly strict emission standards, automobile and catalyst manufacturers have investigated a variety of approaches to reduce cold-start emissions. Attention has been focused on the start-up phase, when 70-80% of the hydrocarbons generated (HCs) by the combustion engine are emitted [1]. Cold-start is referring to the short time period of 1-2 min, after engine ignition and before the three-way catalyst reaches its light-off temperature which is around 200°C. Zeolites have been found to be the preferred molecular sieves and the best candidates for this application due to their stability under a variety of conditions and their affinity to adsorb HCs. In literature, different types of zeolites have been proposed and tested as adsorbents for HC emissions [2]–[11]. It has been reported that ZSM-12, which possesses one dimensional channels with 12-member ring pores, performs better in the envisaged application of hydrocarbon trap compared to more typical three-dimensional zeolites [9]–[14]. With the growing use of one dimensional zeolites in separation and reaction processes, the need to better understand the diffusion and transport properties of molecules within the channels of these materials is important not only from a fundamental, but also from a practical point of view. The mechanism used to describe the simultaneous passage of ethylene (light molecules) and toluene (heavy molecules) inside narrow one dimensional channels was designated as the single-file diffusion[15]. This phenomenon has become a topic of current research interest. Heavy aromatic molecules are strongly adsorbed in the zeolite, therefore they need a higher temperature in order to desorb from channels. On the other hand, light hydrocarbon molecules are more weakly adsorbed and easily desorb from channels at lower temperature. Thus in simultaneous diffusion, the desorption of lighter molecules such as ethylene from one dimensional narrow channels may be retarded by co-adsorbed heavier ones such as toluene.

Despite the large number of theoretical studies published on the single-file diffusion over the years, experimental and numerical single component loading (small molecules or aromatic molecules) are still rare. It is important to understand the transport mechanism of these molecules within the pores of zeolites in order to design more efficient applications for these materials. The aim of this paper is to provide a comparison between experimental and simulation results for each single kind of gas after developing a model for diffusion in zeolite pores.

II. EXPERIMENTAL DETAILS

The detailed synthesis procedure and physicochemical characterization results for Na-ZSM-12 and Ag-ZSM-12 samples with molar ratio Si/Al = 52 used in this research were described in our previous study[15]. Fig. 1 shows the scanning electron micrographs of Na-ZSM-12 and Ag-ZSM-12 zeolites as synthetized samples. They have uniform shape and particle size; crystals have spherical form with average crystal diameter of 1µm related to the use of methyltriethylammonium chloride as organic template. This is agreement with the X-ray diffraction patterns of these hydrocarbon adsorbents that were recorded using a Siemens D5000 diffractometer using the CuKα (λ = 1.54184Å) as shown in Fig. 2.

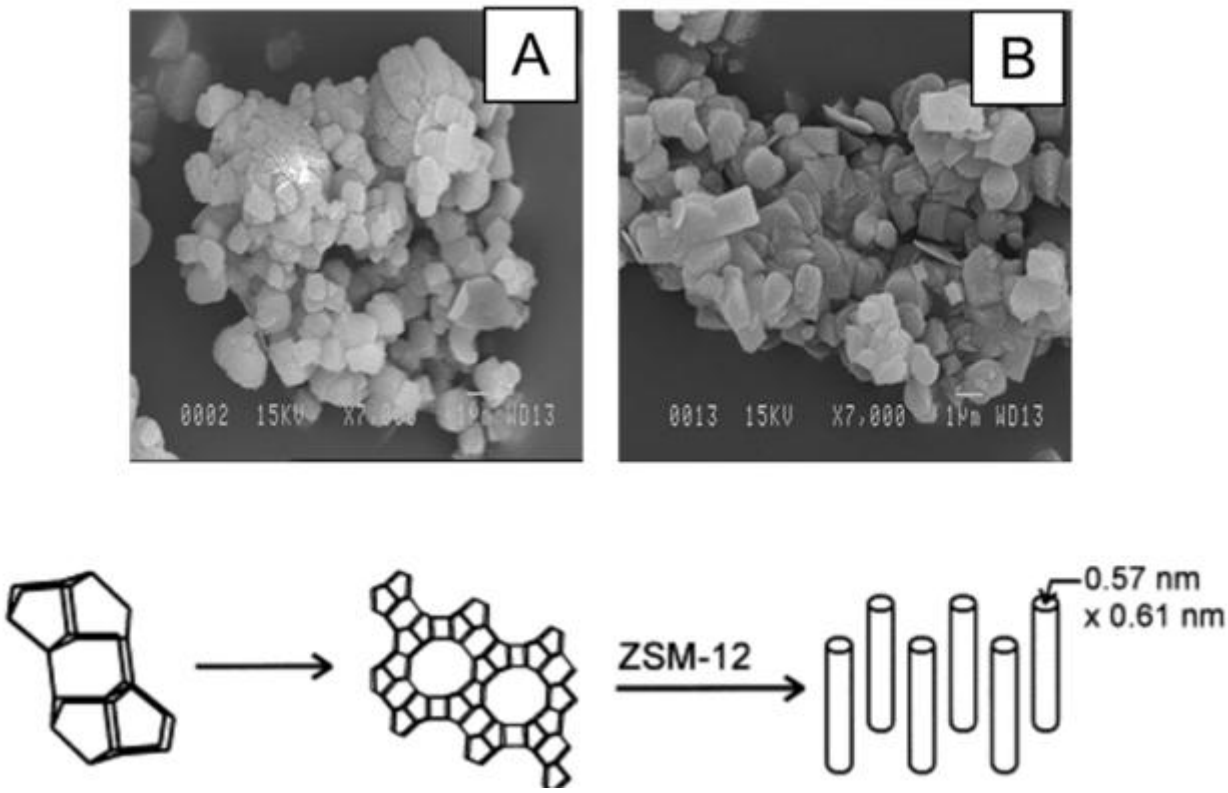

FIG.1. SCANNING ELECTRON MICROGRAPH OF SYNTHESIZED SAMPLE (A) Na-ZSM-12 and (B) Ag-ZSM-12 (52).

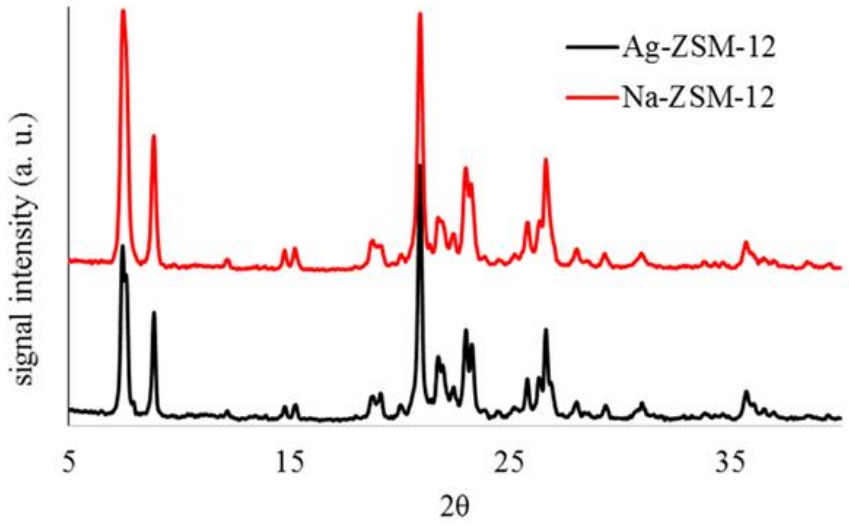

FIG.2. X-RAY POWDER DIFFRACTION PATTERNS OF AS-SYNTHESIZED Ag-ZSM-12 AND Na-ZSM-12 SAMPLES.

The high intensity of the XRD lines and the low background intensity point out that the samples are highly crystalline. The BET surface area and micropore volume were determined using an Omnisorp-100 automatic analyzer after degassing the sample at 150 °C for at least 4h under vacuum (10^{-5} to 10^{-4} Torr). Using Fourier transform infrared spectroscopy of chemisorbed pyridine, Na-ZSM-12 has a higher measured $C_{Brönsted}/C_{Lewis}$ ratio compared to Ag-ZSM-12 indicating larger content of Lewis acid sites. Brönsted and Lewis acid centers are detected respectively by peaks around 1550 cm^{-1} and 1448cm^{-1} (Fig. 3, Table 1). The acid site density of zeolites was quantified by ammonia thermodesorption. All experimental results are reproduced here from our previous work (Table 2)[15].

TABLE 1
FTIR RESULTS OF CHEMISORBED PYRIDINE

Sample	Si/Al	Peak area (a. u.) 1448 cm^{-1}	Peak area (a. u.) 1550 cm^{-1}	$C_{Brönsted}$ / C_{Lewis}
Na-ZSM-12	52	0.012	0.322	35.5
Ag-ZSM-12	52	0.482	0.152	0.42

$$C_{Brönsted}/C_{Lewis} = 1.88*A_{1550} / 1.42*A_{1448}$$ [23]

TABLE 2
NH_3 TPD RESULTS.

Sample	T_{peak1} (°C)	NH_3 (mol/g cat $*10^5$)	T_{peak2} (°C)	NH_3 (mol/g cat $*10^5$)	T_{peak3} (°C)	NH_3 (mol/g cat $*10^5$)
Na-ZSM-12 (52)	92	32	150	13.4	345	204.6
Ag-ZSM-12 (52)	145	38.5	213	131.4	360	64.7

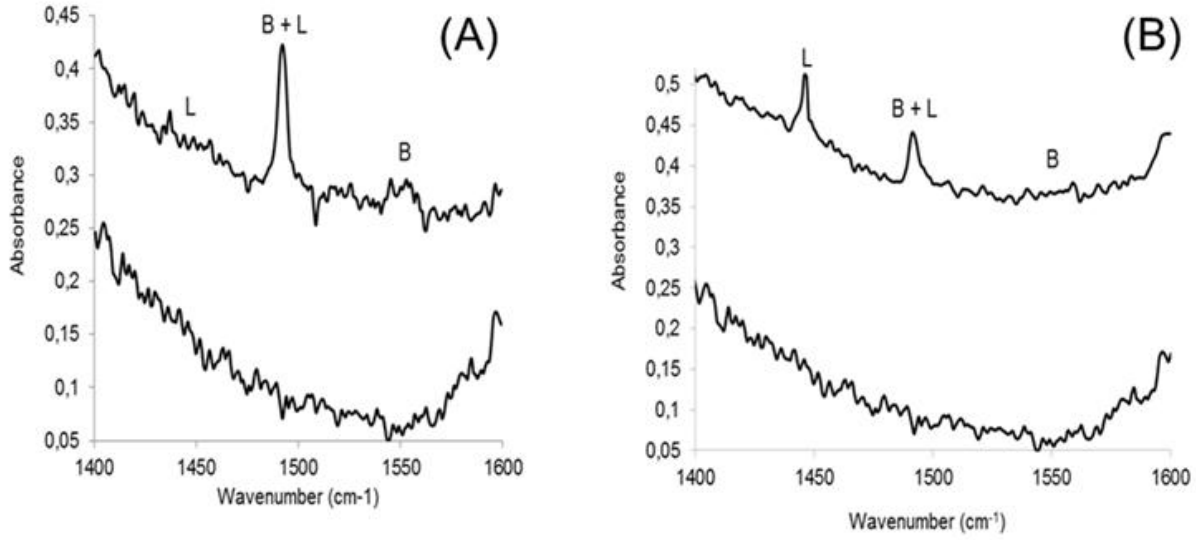

FIG.3 FTIR SPECTRA OF CHEMISORBED PYRIDINE (DESORPTION TEMPERATURE 150°C) OF SAMPLES WITH SI/AL=52; (A) NA-ZSM-12; (B) AG-ZSM-12.

Here we report the application of laser diode thermal desorption (S-960 LDTD) sample introduction source, coupled with an atmospheric pressure chemical ionization (APCI) source mounted on a quantum ultra AM triple quadripole mass spectrometer for analyte detection. This device allows reaching ramping rates similar to those reached in a muffler which is around 3-5°C/s. Samples preliminarily loaded with adsorbed single-component ethylene and toluene separately at room temperature were deposited in the Lazewell plates of the LDTD source (Phytronix).

III. SINGLE-COMPONENT GAS DESORPTION MODELING

3.1 Model description

The desorption process of a single-component gas can be simulated using a transient diffusion boundary value problem coupled with Fick's law [16], [17]. In the present study, due to the structure of Na-ZSM-12and Ag-ZSM-12samples, a one-dimensional diffusion problem is considered[9], [15], [18]. For this purpose, let L and t_{T_f} denote the zeolite sample length

and the total time of the desorption process, respectively. At a given time $t \in \left[0, t_{T_f}\right]$, let $\rho(t, \mathrm{x})$ denotes the gas density at the position $x \in [0, L]$. The transient diffusion problem is given by the following equations [17], [19]:

$$\frac{\partial \rho(t,x)}{\partial t} + div\left(J(t,x)\right) = 0 \ , \ \forall (t,x) \in \left[0, t_{T_f}\right] \times [0, L] \tag{1}$$

$$J(t,x) = -\omega(\mathrm{t}, x) \nabla \rho(t,x) \tag{2}$$

with the Neumann and Dirichlet boundary conditions:

$$\begin{cases} J(x=0,t) = 0 \ , \ \forall t \\ \rho(x=L,t) = 0, \ \forall t \end{cases} \tag{3}$$

and the initial condition:

$$\rho(x, t=0) = \rho_0(x), \ \forall x \in [0, L] \tag{4}$$

In expressions (1)-(2), $div(.)$ and ∇ are divergence and gradient operators, respectively. $J(t,x)$ and $\omega(t,x)$ represent the gas flux and the diffusion coefficient. Substituting the flux expression (2) into the formula (1) leads to the following partial differential equation:

$$\frac{\partial \rho(t,x)}{\partial t} = div\left(\omega(\mathrm{t}, x) \nabla \rho(t,x)\right) \ , \ \forall (t,x) \in \left[0, t_{T_f}\right] \times [0, L] \tag{5}$$

In the sequel, the material is assumed to be homogeneous. Therefore, the diffusion coefficient is only time-dependent and it is defined according to the Arrhenius law [16], [17], [20]:

$$\omega(t) = C \Gamma \exp\left(-\frac{E}{kT}\right) \tag{6}$$

where $E\left(kJ.\mathrm{mol}^{-1}\right)$, $k\left(J.mol^{-1}.K^{-1}\right)$ and $T(K)$ are the activation energy, the Boltzmann constant and the temperature. Γ and C are two constants. Γ is defined as follows [17], [18]:

$$\Gamma = \exp\left(\frac{E}{kT_f}\right) \tag{7}$$

Moreover, during the experiments the temperature is increased according to a constant heating rate λ:

$$T(t) = T_0 + \lambda t \tag{8}$$

where T_0 is the initial temperature.

In some research works [16], [17], [19], [21], it has been shown, through numerical simulations, that the above mentioned diffusion model fails to predict the general shape of the gas flux, especially at the beginning of the desorption process. In order to overcome such a drawback, it has been suggested in the work of Chatterjee el al. [17]–[19]to use two diffusion coefficients: i) the first one defined inside the physical domain and ii) an additional diffusion coefficient defined on the domain boundary with a higher activation energy. Thus, two diffusion coefficients will be considered:

$$\begin{cases} \omega(t) = C_\omega \Gamma_\omega \exp\left(-\dfrac{E_\omega}{kT}\right), \ \forall x \in [0, L[\\ \Xi(t) = C_\Xi \Gamma_\Xi \exp\left(-\dfrac{E_\Xi}{kT}\right), \ if \ \ \mathrm{x} = \mathrm{L} \\ \Gamma_\omega = \exp\left(\dfrac{E_\omega}{kT_f}\right) \\ \Gamma_\Xi = \exp\left(\dfrac{E_\Xi}{kT_f}\right) \\ E_\Xi > E_\omega \end{cases} \tag{9}$$

For more details about this extra-diffusion barrier the reader is referred to the following references [16], [17], [20].

3.2 Time and Space Discretization

The boundary value problem (1)-(5) is solved using the finite difference method [22]. To this end, the spatial domain $[0, L]$ is discretized into a grid of nodes $(x_i)_{i=1}^{NS}$ such that $x_1 = 0$ and $x_{NS} = L$. The time domain $\left[0, t_{T_f}\right]$ is also discretized into a set of time points $(t_j)_{j=0}^{NT}$. Without loss of generality, nodes and time points are supposed equidistant with fixed space step Δx and fixed time step Δt. Therefore, one can show that:

$$\begin{cases} t_j = j \times \Delta t, \ \forall j = 0, .., NT \\ x_i = x_1 + (i-1) \times \Delta x, \ \forall i = 1, .., NS \end{cases} \tag{10}$$

Let denotes by ρ_i^j the approximation of the solution $\rho(t_j, x_i)$ at given time t_j and point x_i. Using a central difference scheme, the right hand term of equation (5) is approximated by the following scheme [22]:

$$div\left(\omega(t_j)\nabla\rho(t_j, x_i)\right) \approx \omega(t_j)\frac{\rho_{i+1}^j - 2\rho_i^j + \rho_{i-1}^j}{(\Delta x)^2} \tag{11}$$

For the time discretization of equation (5) an explicit scheme is used [22] Thus, the time partial derivative is approximated as follows:

$$\frac{\partial\rho(t_j, x_i)}{\partial t} \approx \frac{\rho_i^{j+1} - \rho_i^j}{\Delta t} \tag{12}$$

Combining expressions (11)-(12) leads to the following finite difference approximation scheme:

$$\rho_i^{j+1} = \rho_i^j + \omega(t_j)\frac{\Delta t}{(\Delta x)^2}\left(\rho_{i+1}^j - 2\rho_i^j + \rho_{i-1}^j\right) \tag{13}$$

Therefore, knowing the solution at time step t_j, the solution is updated in a straightforward way for the time step t_{j+1}. In expression (13) the time step Δt is considered small enough compared to the square of the space step Δx in order to fulfill the stability condition for the explicit scheme [22].

IV. EXPERIMENTAL AND NUMERICAL RESULTS

4.1 Experimental results

In our previous study using Fourier transform infrared spectroscopy of chemisorbed pyridine characterization, it has been shown that Ag-ZSM-12 has low measured $C_{Brönsted}/C_{Lewis}$ indicating largest content of Lewis acid sites. On the other hand, Na-ZSM-12 has a lower 1448 cm^{-1} peak area, a characteristic band of Lewis acid centers, than Ag-ZSM-12. Consequently the ration $C_{Brönsted}/C_{Lewis}$ for Na-ZSM-12 increased. The Ag exchanged zeolite has the highest content in Lewis acid sites and the lowest content in Brönsted acid sites (lowest 1550 cm^{-1} peak area)[15].

Three high heating rates have been used for the desorption process: 3°C/s, 5°C/s and 9°C/s. Fig.4 reports TPD profiles of the single-component, either ethylene and toluene, from Na-ZSM-12 and Ag-ZSM-12. All desorption profiles of both ethylene and toluene display a single peak, except for the desorption curves of ethylene from Ag-ZSM-12 (Fig.5), which show two peaks. In the latter case the low temperature peak is assigned to the ethylene desorption from Brönsted acid sites whereas the high temperature desorption peak is from Lewis acid centers.

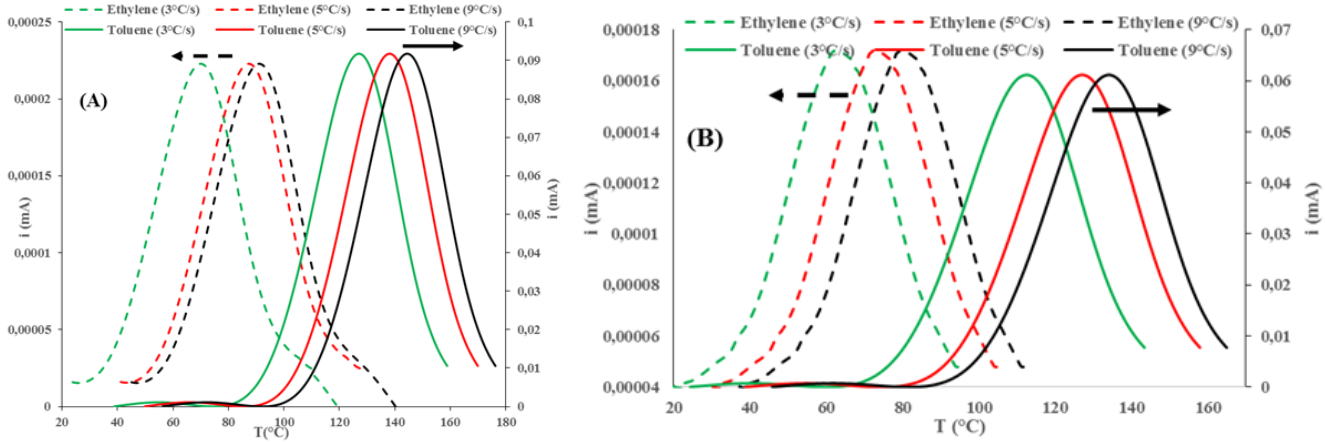

FIG.4. SINGLE COMPONENT (ETHYLENE OR TOLUENE) TPD PROFILES OF (A) Na-ZSM-12 AND (B) Ag-ZSM-12 SAMPLES AT DIFFERENT HEATING RATES.

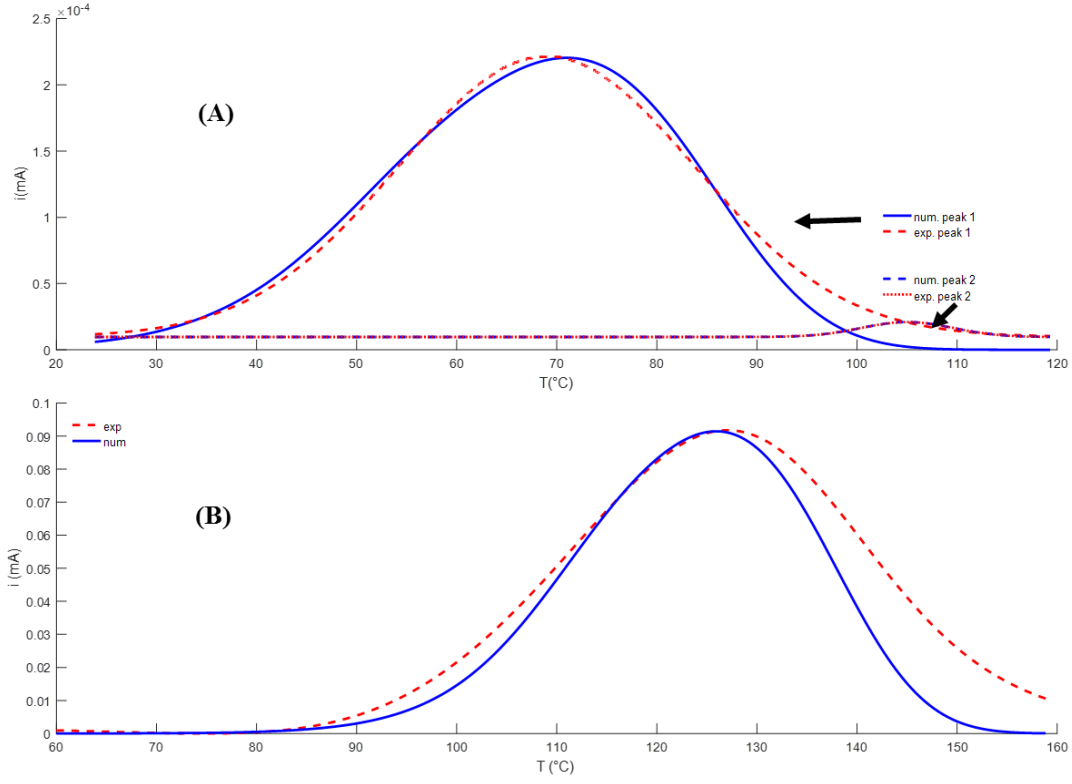

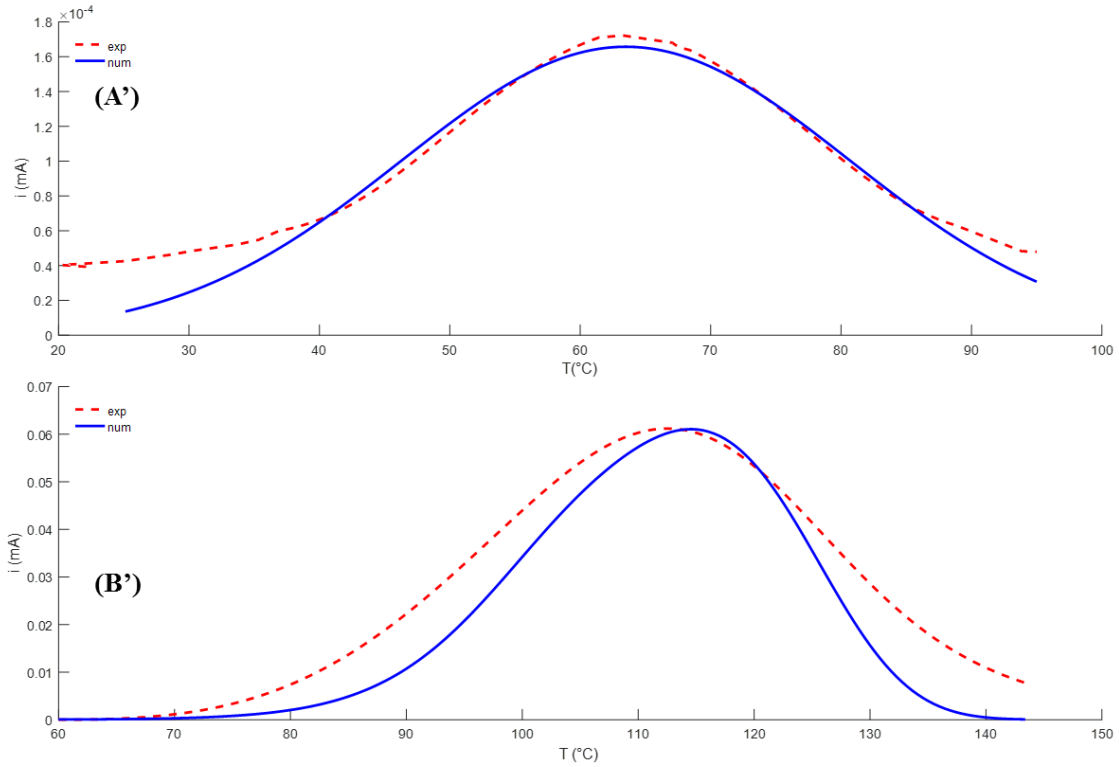

FIG.5. COMPARISON OF EXPERIMENTAL AND NUMERICAL DATA OF SINGLE-COMPONENT TPD PROFILES IN AG-ZSM-12: (A) ETHYLENE AND (B) TOLUENE AND NA-ZSM-12: (A') ETHYLENE AND (B') TOLUENE WITH 3°C/S AS HEATING RATE. VALUES OF E_w AND E_Ξ REPORTED IN TABLE 4 WERE USED WITH $\Gamma_w = \exp\left(\frac{E_w}{kT_f}\right)$ and $\Gamma_\Xi = \exp\left(\frac{E_\Xi}{kT_f}\right)$.

According to Table 3 the amounts of both ethylene and toluene detected are essentially not affected by the heating rate which is an indication of results reproducibility. However a clear dependence of desorption temperature on heating rate for toluene and ethylene was observed for the two zeolites. At increasing ramp rate from 3 to 9°C, the maximum desorption peak temperature is raised by 10-25°C. Regarding the desorption temperature of both ethylene and toluene molecules, it seems that the desorption temperature of Na-ZSM-12 is always lower than the desorption temperature of Ag-ZSM-12. This result emphasizes the importance of the strong Lewis acid sites in Ag-ZSM-12 and confirms that the zeolite exchanged with Ag^+ is a better candidate as hydrocarbon adsorbent as indicated by its higher desorption temperatures [9], [15].

TABLE 3
SINGLE COMPONENT TPD RESULTS

Gas	Rate (°C/s)	Desorbed amounts (mmol/g)		Desorption temperature (°C)	
		Na-ZSM-12	*Ag-ZSM-12*	*Na-ZSM-12*	*Ag-ZSM-12*
Ethylene	*3*	0.021	0.042	63	(70*;105**)
	5	0.023	0.044	73	(81*;114**)
	9	0.020	0.042	80	(89*;126**)
Toluene	*3*	1.73	1.94	112	126
	5	1.71	1.92	126	137
	9	1.72	1.95	133	144

**Desorption temperature obtained from the low T peak*
***Desorption temperature obtained from the high T peak*

Independently of the zeolite and heating rate, the amount of toluene adsorbed and the desorption temperature are much higher than those of ethylene.This indicates that part of ethylene is either not adsorbed at all or so weakly adsorbed that it is desorbed at room temperature. It is found that toluene is more strongly adsorbed than ethylene on both Brönsted and Lewis acid sites[15]. As shown in Table3, the amount of ethylene adsorbed on Ag-ZSM-12 is higher than the amount adsorbed on Na-ZSM-12 which also indicates that the silver form is a better adsorbent for the smaller gas molecules.

4.2 Numerical results

In order to show the ability of the transient diffusion boundary value problem (1)-(2) to predict the obtained experimental results, numerical simulations were carried out using the finite difference method (13). As mentioned earlier, two diffusion coefficients will be considered for each gas (9). The ZSM-12 zeolite has a typical channel length nearly equal to $5\mu m$ and a pore size of $5.7 \times 6.1 \overset{\circ}{A}$. Molecular diameters of ethylene and toluene are $1.4 \overset{\circ}{A}$ and $5.7 \overset{\circ}{A}$, respectively.

In Fig. 5 (A' and B'), numerical simulation results for ethylene and toluene desorption process using Na-ZSM-12 zeolite are compared to experimental trends. It is shown that the diffusion model predicts desorption curves in a good agreement with experimental results. Values of the activation energy used for these simulations are reported in Table 4. For the three heating rates, activation energies associated to the ethylene are smaller than those of toluene. This trend could be explained through the dimension of ethylene molecule which is smaller compared to the dimension of zeolite channels, in contrast to the toluene molecule. As a consequence, ethylene can desorb with a lower energy of activation. For both gases and for all heating rates the activation energy inside the domain (E_ω) is lower than the activation energy at the lattice boundary (E_Ξ). Such a result corroborates the hypothesis made in Chatterjee et al.[17] Suggesting the introduction of an additional activation energy at the boundary. Furthermore, we notice that increasing the heating rate leads to decreasing activation energy (see Table 4). Indeed, by increasing temperature, the cages of zeolite channels undergo higher vibration and thermal agitation which allows the adsorbed hydrocarbon molecules to be diffuse more easily.

TABLE 4
ACTIVATION ENERGY OBTAINED FROM NUMERICAL PROGRAM (kJ.mol^{-1})

Sample	Rate (°C/s)	Ethylene			Toluene		
		E_w	E_Ξ	T_f (K)	E_w	E_Ξ	T_f (K)
Na-ZSM-12	3	77	129	369	84	184	416
	5	70	120	378	80	180	431
	9	61	110	385	75	175	438
Ag-ZSM-12	3	(50^{*}; 105^{**})	(114^{*}; 410^{**})	391	88	187	431
	5	(43^{*}; 73^{**})	(111^{*}; 388^{**})	410	85	185	443
	9	(34^{*}; 55^{**})	(107^{*}; 350^{**})	413	75	180	449

* ***Activation energy value obtained from the low T peak***
** ***Activation energy value obtained from the high T peak***

For the Ag-ZSM-12 zeolite, numerical and experimental results for the desorption process are compared in Fig. 6. Since ethylene desorption curves (Fig. 6 (A)) exhibit two peaks corresponding, respectively, to Brönsted acid sites (low temperature peak) and Lewis acid centers (high temperature peak), a deconvolution operation was carried out using FitPeak Matlab code in order to uncouple peaks (Fig. 6). Fig. 5 (A and A') show a benchmark between numerical and experimental results for the ethylene at 3°C/s as an example of a heating rate while Fig. 5 (B and B') illustrate results for toluene. It is shown that numerical results are in a good agreement with experimental trends. The activation energy values used in Equations (9) and (11) for the Ag-ZSM-12 zeolite are reported in Table 4. The aforementioned remarks about the Na-ZSM-12 zeolite, namely: i) ethylene having activation energy lower than toluene, ii) activation energy inside the zeolite lower than the activation energy at the lattice boundary and iii) decreasing activation energy at increasing heating rate, still hold for the Ag-ZSM-12 zeolite.

Finally, it may be concluded that, for both ethylene and toluene, activation energies for Na-ZSM-12 are lower than those of Ag-ZSM-12 (see Table 4). This can be explained by the presence of strong Lewis acid sites in Ag^+ exchanged zeolite while the Na-ZSM-12 zeolite is characterized by the presence of mainly Brönsted acid sites.

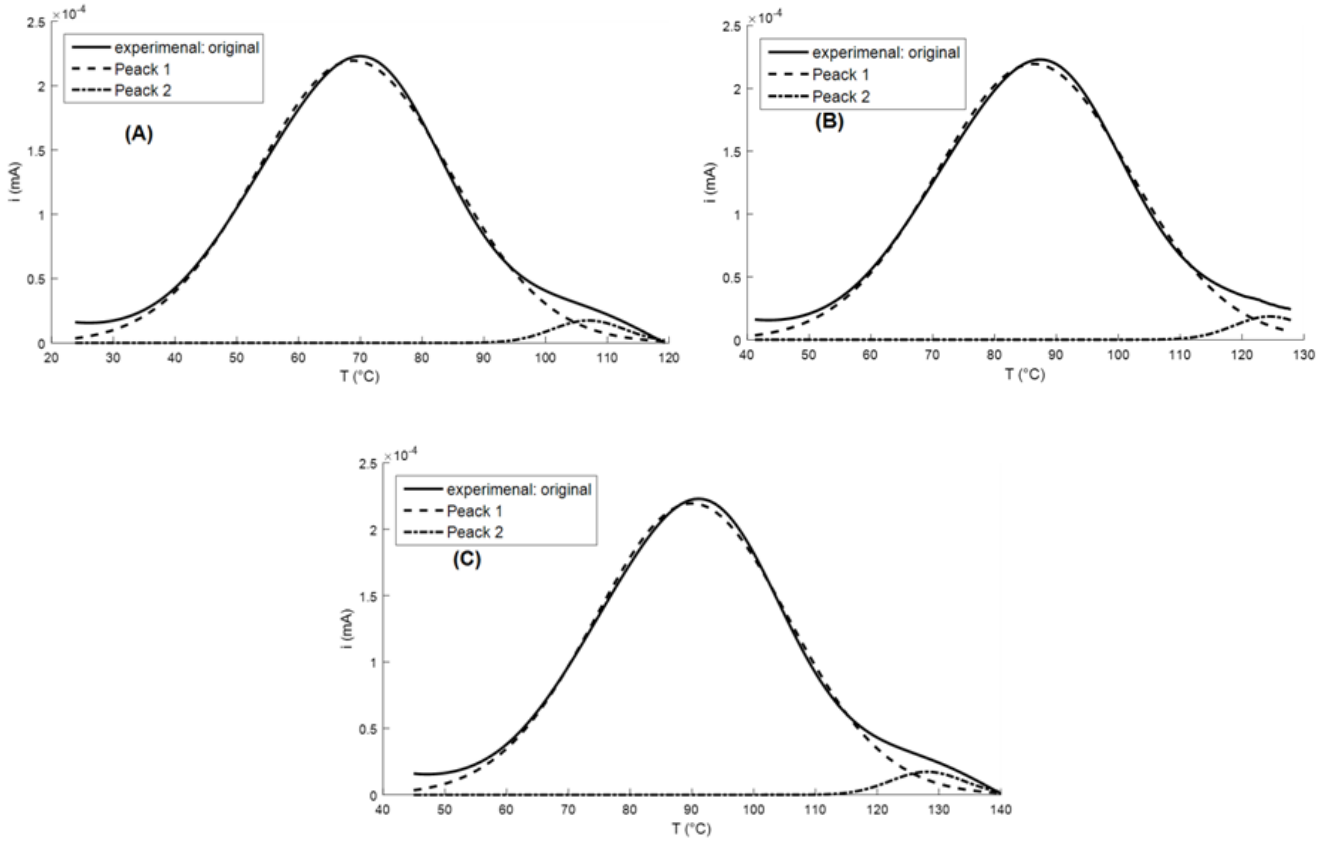

FIG.6. ETHYLENE THERMODESORPTION PROFILE OF AG-ZSM-12 WITH (A) 3°C/s, (B) 5°C/s AND (C) 9°/s HEATING RATE

V. CONCLUSION

Diffusion of a single adsorbed component ethylene or toluene, inside the microporous ZSM-12 zeolite was studied experimentally and numerically. The Na^+ and Ag^+ forms of zeolite ZSM-12 were synthetized and characterized. The thermodesorption process was conducted at three different heating rates (3, 5 and 9°C/s) selected to be similar to the muffler heating rate during the cold start process.

Experimentally, it was verified that the amount of both ethylene and toluene detected are essentially not affected by the heating rate. Contrary to the ethylene adsorbed on Ag-ZSM-12, where this molecule desorbed as two peaks, only one peak was observed for toluene. Moreover the amounts of ethylene adsorbed on ZSM-12 are low compared to those of toluene, due to the small size of this molecule in comparison to the pore diameter of this zeolite adsorbent.

Numerically, using a transient diffusion boundary value problem coupled with Fick's law, it was possible to explain all qualitative features of the temperature dependent desorption profiles observed experimentally. In this model, a coefficient C was included in the diffusion coefficient $\omega(t)$ (6) that has units of m^2/s and consequently the term $\rho(t,x)$ which describes the probability that a molecule occupies a site at distance x in the zeolite channels at time t is dimensionless.

For the two solids considered in this study, activation energies E_w and E_Ξ for toluene are much higher than those for ethylene owing to its bigger size. We have also shown that the values of these parameters are higher for the Ag^+ exchanged zeolite than for Na-ZSM-12 because of the presence of strong Lewis acid sites in the former material. In addition each

activation energy for Na-ZSM-12 and Ag-ZSM-12 decreases at increasing heating rate. This was explained by thermal vibrations of lattice which allow higher diffusivity at high temperature.

ACKNOWLEDGEMENTS

The authors gratefully acknowledge Natural Science and Engineering Research Council of Canada for financial support.

REFERENCES

[1] F. F. Zhao, *Technologies for Near-Zero-Emission Gasoline-Powered Vehicles*. 2006.
[2] S. P. Elangovan, M. Ogura, S. Ernst, M. Hartmann, S. Tontisirin, M. E. Davis, and T. Okubo, "A comparative study of zeolites SSZ-33 and MCM-68 for hydrocarbon trap applications," *Microporous Mesoporous Mater.*, vol. 96, pp. 210–215, 2006.
[3] S. P. Elangovan, M. Ogura, M. E. Davis, and T. Okubo, "SSZ-33: A promising material for use as a hydrocarbon trap," *J. Phys. Chem. B*, vol. 108, no. 35, pp. 13059–13061, 2004.
[4] P. Brauer, J. Karger, and N. Neugebauer, "Reaction and Particle Distribution in Networks of Single-File Systems," *Europhys. Lett.*, vol. 53, no. 1, pp. 8–14, 2001.
[5] J. M. López, M. V. Navarro, T. García, R. Murillo, a. M. Mastral, F. J. Varela-Gandía, D. Lozano-Castelló, a. Bueno-López, and D. Cazorla-Amorós, "Screening of different zeolites and silicoaluminophosphates for the retention of propene under cold start conditions," *Microporous Mesoporous Mater.*, vol. 130, no. 1–3, pp. 239–247, 2010.
[6] B. Puértolas, M. Navlani-García, J. M. López, T. García, R. Murillo, a. M. Mastral, M. V. Navarro, D. Lozano-Castelló, a. Bueno-López, and D. Cazorla-Amorós, "Molecular simulation design of a multisite solid for the abatement of cold start emissions," *Chem. Commun.*, vol. 48, p. 6571, 2012.
[7] K. F. Czaplewski, T. L. Reitz, Y. J. Kim, and R. Q. Snurr, "One-dimensional zeolites as hydrocarbon traps," *Microporous Mesoporous Mater.*, vol. 56, no. 1, pp. 55–64, 2002.
[8] S. Gopal, K. Yoo, and P. G. Smirniotis, "Synthesis of A1-rich ZSM-12 using TEAOH as template," *Microporous Mesoporous Mater.*, vol. 49, no. 1–3, pp. 149–156, 2001.
[9] Z. Sarshar, M. H. Zahedi-Niaki, Q. Huang, M. Eić, and S. Kaliaguine, "MTW zeolites for reducing cold-start emissions of automotive exhaust," *Appl. Catal. B Environ.*, vol. 87, no. 1–2, pp. 37–45, 2009.
[10] A. Iliyas, Z. Sarshar, H. M. Zahedi-Niaki, M. Eić, and S. Kaliaguine, "One-dimensional molecular sieves for hydrocarbon cold start emission control," *Top. Catal.*, vol. 52, pp. 1860–1867, 2009.
[11] Z. Sarshar, M. H. Zahedi-Niaki, Q. Huang, and S. Kaliaguine, "Synthesis, structural and acidity characterizations of the large-pore zeolite SSZ-42 for controlling cold-start emissions," *Microporous Mesoporous Mater.*, vol. 118, no. 1–3, pp. 373–381, 2009.
[12] A. Iliyas, M. Eic, M. H. Zahedi-Niaki, and S. Vasenkov, "Toward observation of single-file diffusion using the tracer zero-length column method," *J Phys Chem B*, vol. 112, no. 12, pp. 3821–3825, 2008.
[13] A. Iliyas, M. H. Zahedi-Niaki, M. Eić, and S. Kaliaguine, "Control of hydrocarbon cold-start emissions: A search for potential adsorbents," *Microporous Mesoporous Mater.*, vol. 102, no. 1–3, pp. 171–177, 2007.
[14] A. Iliyas, H. M. Zahedi-Niaki, and M. Eić, "One-dimensional molecular sieves for hydrocarbon cold-start emission control: Influence of water and CO2," *Appl. Catal. A Gen.*, vol. 382, no. 2, pp. 213–219, 2010.
[15] I. Daldoul, S. Auger, P. Picard, B. Nohair, and S. Kaliaguine, "Effect of temperature ramp on hydrocarbons desorption profiles from zeolite ZSM-12.," *Can. J. Chem. Eng.*, vol. 94, article in press, 2015.
[16] J. Kärger, R. Valiullin, and S. Vasenkov, "Molecular dynamics under confinement to one dimension: Options of measurement and accessible information," *New J. Phys.*, vol. 7, pp. 1–15, 2005.
[17] S. Chatterjee and G. M. Schütz, "Diffusion of a hydrocarbon mixture in a one-dimensional zeolite channel: An exclusion model approach," *Microporous Mesoporous Mater.*, vol. 125, no. 1–2, pp. 143–148, 2009.
[18] S. Chatterjee and G. M. Schütz, "Diffusion of a hydrocarbon mixture in a one-dimensional zeolite channel: An exclusion model approach," *Microporous Mesoporous Mater.*, vol. 125, no. 1–2, pp. 143–148, Oct. 2009.
[19] S. Chatterjee and G. M. Schütz, "Diffusion in a One-Dimensional Zeolite Channel : An Analytical and Numerical Study," *Diffusion-Fundamentals.Org*, vol. 11, no. 2009, pp. 1–13, 2009.
[20] J. Karger, M. Petzold, H. Pfeifer, S. Ernst, and J. Weitkamp, "Single-file diffusion and reaction in zeolites," *J. Catal.*, vol. 136, no. 2, pp. 283–299, 1992.
[21] P. Bräuer, A. Brzank, and J. Kärger, "Adsorption and Reaction in Single-File Networks," *J. Phys. Chem. B*, vol. 107, no. 2, pp. 1821–1831, 2003.
[22] N. Ozisik, *Finite Difference Methods in Heat Transfer*, CRC Press,. 1994.